



Postglacial fluctuations of Cordillera Darwin glaciers (southernmost Patagonia) reconstructed from Almirantazgo fjord sediments



Sebastien Bertrand ^{a, b, *}, Carina B. Lange ^{c, d}, Silvio Pantoja ^c, Konrad Hughen ^b, Evi Van Tornhout ^a, Julia Smith Wellner ^e

^a Renard Centre of Marine Geology, Ghent University, Ghent, Belgium

^b Marine Chemistry and Geochemistry, Woods Hole Oceanographic Institution, MA, USA

^c Department of Oceanography and COPAS Sur-Austral Center, Universidad de Concepción, Concepción, Chile

^d FONDAP-IDEAL Center, Universidad Austral de Chile, Valdivia, Chile

^e Department of Earth and Atmospheric Sciences, University of Houston, TX, USA

ARTICLE INFO

Article history:

Received 13 July 2017

Received in revised form

15 October 2017

Accepted 18 October 2017

Keywords:

Fjord sediments
Ice-rafted debris
Meltwater
Neoglaciation
Holocene

ABSTRACT

Most outlet glaciers of the Cordillera Darwin Icefield (CDI; Patagonia, 54°S) are currently transitioning from calving to land-based conditions. Whether this situation is unique to the modern climate or also occurred during the Holocene is entirely unknown. Here, we investigate the Holocene fluctuations of outlet glaciers from the northern flank of the CDI using a multi-proxy sedimentological and geochemical analysis of a 13.5 m long sediment core from Almirantazgo fjord. Our results demonstrate that sedimentation in Almirantazgo fjord started prior to 14,300 cal yr BP, with glacier-proximal deposits occurring until 13,500 cal yr BP. After 12,300 cal yr BP, most glaciers had retreated to land-locked locations and by 9800 cal yr BP, Almirantazgo fjord was a predominantly marine fjord environment with oceanographic conditions resembling the present-day setting. Our sediment record shows that during the first part of the Holocene, CDI glaciers were almost entirely land-based, with a possible re-advance at 7300–5700 cal yr BP. This is in clear contrast with the Neoglaciation, during which CDI glaciers rapidly re-advanced and shrank back several times, mostly in phase with the eastern outlet glaciers of the Southern Patagonian Icefield (SPI). Two significant meltwater events, indicative of rapid glacier retreat, were identified at 3250–2700 and 2000–1200 cal yr BP, based on an increase in grain-size mode and related inorganic geochemical parameters. This interpretation is additionally supported by concomitant decreases in organic carbon of marine origin and in Cl counts (salinity), reflecting higher terrestrial input to the fjord and freshening of the fjord waters. Overall, our record suggests that CDI outlet glaciers advanced in phase with eastern SPI glaciers during the Neoglaciation, and retreated far enough into their valleys twice to form large outwash plains. Our results also highlight the potential of fjord sediments to reconstruct glacier variability at high resolution on multi-millennial timescales.

© 2017 Elsevier Ltd. All rights reserved.

1. Introduction

Patagonian glaciers are among the fastest retreating ice masses on Earth (Lemke et al., 2007). The reasons behind this exceptional retreat during the last few decades are frequently debated in the literature but they generally include a complex combination of increasing atmospheric temperature, decreasing precipitation, and accelerated calving (Rignot et al., 2003; Glasser et al., 2011), locally

enhanced by wind-driven intrusions of warm ocean waters (Moffat, 2014). To better understand Patagonian glacier-climate relationships on longer, i.e., centennial, timescales, it is necessary to develop continuous records of glacier mass balance that extend beyond instrumental timescales. Several such glacier variability reconstructions were recently produced for the Northern (NPI) and Southern (SPI) Patagonian Icefields (e.g., Glasser et al., 2004; Bertrand et al., 2012a; Strelin et al., 2014). Comparatively, very few records exist for the glaciers of the southernmost Cordillera Darwin Icefield (CDI; Kuylenstierna et al., 1996; Strelin et al., 2008). The reason for this lack of southernmost records is largely related to the morphodynamic setting of most CDI glaciers, i.e., they are fjord-

* Corresponding author. Renard Centre of Marine Geology, Ghent University, Ghent, Belgium.

E-mail address: sebastien.bertrand@ugent.be (S. Bertrand).

terminating, which results in very limited terrestrial evidence of glacier variability.

The existence of glaciers reaching sea level in Patagonia is mostly due to the very high precipitation that characterizes the area, which reflects the interruption of the westerly flow of humid air by the southern Andes (Garreaud et al., 2013). Given the mostly W-E orientation of Cordillera Darwin compared to the pure N-S orientation of the NPI and SPI (Fig. 1), CDI glaciers may respond very differently to changes in westerly wind-driven precipitation and results obtained on NPI and SPI glaciers cannot simply be extrapolated to CDI glaciers. Yet, CDI glaciers are the least studied of all Patagonian glaciers (Lopez et al., 2010). Reconstructing the fluctuations of CDI glaciers during the Holocene is therefore critically needed to obtain a more comprehensive understanding of the relation between climate and glacier variability in Patagonia.

Techniques traditionally used to reconstruct glacier variability, i.e., geomorphic mapping and exposure dating, are of relatively little use in Cordillera Darwin since most CDI glaciers are calving into fjords. This morphodynamic characteristic however offers the possibility to use the sediments from the fjords in which these glaciers calve to reconstruct glacier fluctuations (e.g., Howe et al., 2010; Andresen et al., 2011; Bertrand et al., 2012a). Compared to the traditional geomorphic and exposure dating approach, which provides notoriously discontinuous records of maximum ice extent, fjord sediments offer the advantage of holding continuous records of both glacier advance and retreat. They are particularly useful to detect calving/land-based transitions, based on the concentrations of ice-rafted debris (IRD), for example (Andresen et al., 2011; Kuijpers et al., 2014).

Although fjord sediments contain a huge potential for glacier mass balance reconstructions in the southern Andes, the number of records from the Patagonian fjords remains very limited (e.g., Boyd et al., 2008; Bertrand et al., 2012a). In addition, most of the existing

work on proglacial fjord sediments in Chilean Patagonia focuses on the deglaciation (Boyd et al., 2008) and/or on quantifying erosion rates (Koppes et al., 2009, 2015; Fernandez et al., 2011). Very little attention has been paid to glacier variations recorded in Holocene fjord sediments.

Here, we use a sediment core from Almirantazgo fjord (54°S) to reconstruct the fluctuations of outlet glaciers from the northern flank of the CDI during the Holocene. Although our sediment core has previously been studied by Boyd et al. (2008), these authors focused on the deglaciation and they concluded that “during the Holocene, stable ice conditions persisted until the mid-1960s”. In contrast, we use a detailed multi-proxy sedimentological and geochemical approach to provide evidence that CDI glaciers shrank and re-advanced several times during the Holocene, mostly in phase with eastern SPI glaciers.

2. Setting

Cordillera Darwin holds the third largest temperate icefield in the Southern Hemisphere. It is located at 54.4–55°S (Fig. 1) and it is composed of 627 glaciers that cover a total area of 2333 km² (Bown et al., 2014). The ice fronts of most CDI outlet glaciers reach sea level and a large fraction of CDI glaciers are currently transitioning from calving to land-based conditions (Porter and Santana, 2003). The icefield is currently losing about 4.3 km³ of ice/year, mostly due to the rapid thinning of glaciers on the northern side (Melkonian et al., 2013). Since the Little Ice Age (LIA), it has lost a total area of 306 km² (Davies and Glasser, 2012). Despite recent retreat throughout the area, nearly half of the CDI glaciers were either stationary or slightly advancing during the last decades (Holmund and Fuenzalida, 1995; Lopez et al., 2010; Davies and Glasser, 2012; Bown et al., 2014), reflecting the dynamic responses of different glaciers in the region.

The largest and most documented glacier of the CDI by far is

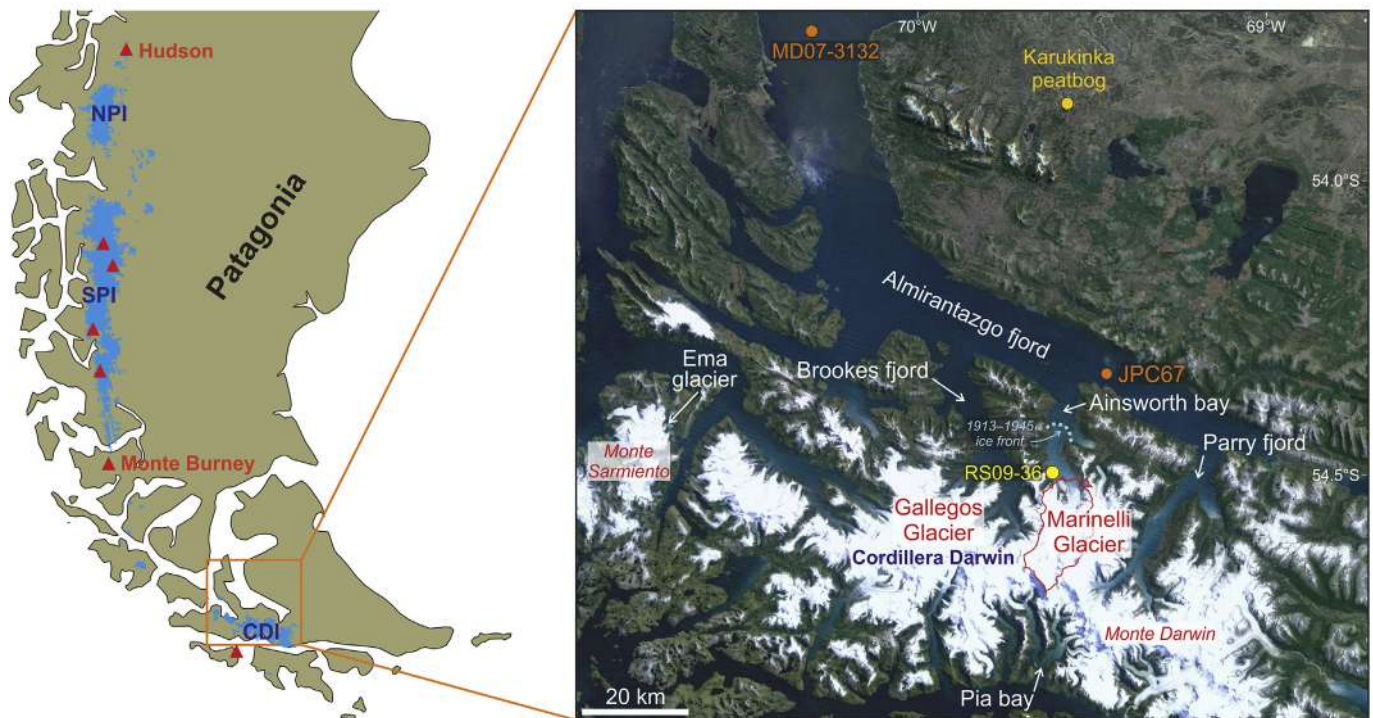


Fig. 1. Location of sediment core JPC67 in Almirantazgo fjord. The other records discussed in the paper are also indicated: sediment core MD07-3132 (Aracena et al., 2015); Karukinka peatbog (Vanneste et al., 2016); Pia bay (Kuylenstierna et al., 1996) and Ema glacier (Strelin et al., 2008). The yellow circle labeled RS09-36 represents a river sediment sample collected in the outwash plain of the western branch of Marinelli glacier (see Appendix 1). NPI: Northern Patagonian Icefield; SPI: Southern Patagonian Icefield; CDI: Cordillera Darwin Icefield. (For interpretation of the references to colour in this figure legend, the reader is referred to the web version of this article.)

Marinelli (Fig. 1), which has a total area of 133 km² and a length of 21 km (Bown et al., 2014). Between 1913 and 2011, Marinelli glacier experienced a frontal retreat of 15 km, most of which occurred after 1945 (Porter and Santana, 2003; Koppes et al., 2009; Bown et al., 2014). Between 1913 and 1945, the relatively stable ice front terminated near the arcuate moraine visible in satellite images (Fig. 1; Porter and Santana, 2003). The atypical rapid retreat of Marinelli glacier during the last decades is mostly due to the geometry of the fjord sub-basins, which resulted in a slow retreat when the glacier was grounded until ~1967, and was followed by a rapid retreat once the glacier became detached from its pinning point (Fig. 1; Koppes et al., 2009).

Cordillera Darwin is located in the present-day core of the southern westerlies (Garreaud et al., 2013). It receives uniform precipitation throughout the year (Sagredo and Lowell, 2012), which can reach up to 5000 mm/yr on top of the icefield (PRECIS-DGF model from Garreaud et al., 2013; RACMO2 model from Lenaerts et al., 2014). The mean annual temperature at sea level reaches 5 °C, with extremes of 8 °C in summer (Feb–Mar) and 1.8 °C in winter (Aug; PRECIS-DGF model). According to Holmlund and Fuenzalida (1995) and Lopez et al. (2010), the E–W orientation of the CDI leads to an orographic effect with greater precipitation on southern and western glaciers and drier and warmer conditions around northern and eastern glaciers. This difference is however not clearly resolved by the most recent high-resolution climate models (Lenaerts et al., 2014).

Most of the northeastern CDI glaciers discharge into Almirantazgo fjord, generally via smaller intermediate fjords, such as Brookes fjord, Ainsworth Bay, and Parry fjord, from North to South (Fig. 1). Almirantazgo fjord therefore receives meltwater from several glaciers, including Gallegos, Marinelli, and the many small glaciers that reach Parry fjord (Fig. 1). As a result, the surface waters of Almirantazgo fjord are slightly brackish (<30 PSU) and flow towards the Northwest (Valdenegro and Silva, 2003). The fjord bathymetry reaches 300 m in front of Ainsworth Bay, and it deepens towards the Northwest to reach values > 500 m at 54°S (SHOA, 1998). The bedrock lithology under the CDI is dominated by Paleozoic metamorphic rocks, with secondary occurrences of Cretaceous granitoids and Jurassic gneiss (Sernageomin, 2003).

Almirantazgo fjord was entirely glaciated during the Last Glacial Maximum. It became ice-free either after advance E (15,500–11,700 cal yr BP; McCulloch et al., 2005) or about 3000 years earlier, i.e. during Henrich Stadial 1 (HS1; 18,000–14,600 cal yr BP) according to Hall et al. (2013). The latter authors argue that the ice had retreated into Ainsworth bay by 16,800 cal yr BP. This early retreat seems to be in agreement with the seismic interpretation of Fernandez et al. (2017), who debate the very existence of glacier advance E, and with the data of Boyd et al. (2008), who show that Marinelli glacier had retreated into Ainsworth Bay before 12,500 cal yr BP, and reached a stable position near its 1945 terminus by 12,500 cal yr BP.

3. Material and methods

In 2005, a 13.45 m long Jumbo Piston Core (JPC67) was collected at a depth of 297 m in Almirantazgo fjord (54.319°S – 69.463°W; Fig. 1) during cruise NBP0505 on board the RVIB Nathaniel B. Palmer. The core was split and described onboard and one half was sub-sampled every 10 cm. The other half was later scanned on a Geotek MSCL core logger (2 cm resolution) at the Antarctic Research Facility (ARF, Florida State University, USA) and on an ITRAX XRF core scanner (Cox Analytical Instruments) at the Woods Hole Oceanographic Institution (MA, USA) at a resolution of 2 mm. The XRF scanner was operated with 20 s scan times using a Mo X-Ray tube set to 30 kV and 45 mA. Additionally, the core was X-

radiographed at the ARF and shell fragments were sampled for radiocarbon analysis. Subsequent measurements were made on the freeze-dried sub-samples taken every 10 cm. These measurements included grain size, ice-rafted debris content, mass-specific magnetic susceptibility, inorganic geochemistry, bulk organic geochemistry, and alkenone sea surface temperature.

Grain size was measured on the terrigenous fraction of the sediment using a Malvern Mastersizer 3000 laser grain size analyzer equipped with a Hydro MV dispersion unit. To isolate the terrigenous fraction, samples were treated with boiling H₂O₂, HCl and NaOH to remove organic matter and possible carbonates and biogenic silica, respectively. Prior to analysis, samples were boiled with sodium pyrophosphate (Na₄P₂O₇ · 10H₂O) to ensure complete disaggregation of the particles. The grain size distribution of the samples was measured during 12 s intervals and the mode of the distributions was computed from the Mastersizer v3.5 software. We used the mode of the grain-size distributions instead of the mean to avoid the influence of ice-rafted debris.

Ice-Rafted Debris (IRD) was quantified using the relative percentage of particles >150 μm following Caniupán et al. (2011). The >150 μm particles were separated by wet-sieving after removal of carbonates with 10% acetic acid and organic matter with 3.5% hydrogen peroxide. IRD was counted from the >150 μm carbonate-free fraction, assuming that coarser-grained terrigenous sediment can only reach the core location through iceberg transport. Given the relative proximity of the glacier fronts to coring site JPC67, we opted for >150 μm instead of the sometimes used >63 μm fraction. Five (0–670 cm) or 10 g (670 cm – bottom) of freeze-dried sediment was used for analysis. As an alternative and independent way of quantifying IRD concentrations, pebbles (>2 mm) present within 5 cm intervals were visually counted on the X-radiographs (Grobe, 1987; data previously published in Boyd et al., 2008). Both IRD estimates are used to assess the presence of nearby calving glaciers (Andrews, 2000).

Mass-specific magnetic susceptibility (MS) was measured with a Bartington MS2G single-frequency (1.3 kHz) sensor, connected to a Bartington MS3 meter. Sediment samples were gently packed into 1 ml LDPE vials and were analyzed in duplicate. The MS values were divided by the sample weight to obtain mass-specific MS values.

For bulk organic geochemistry, approximately 50 mg of sediment was weighed in tin capsules, treated with 1N sulphurous acid to remove possible carbonates (Verardo et al., 1990) and analyzed at the UC Davis Stable Isotope Facility. Total Organic Carbon (TOC) and the carbon stable isotopic ratio (δ¹³C) were measured by continuous flow isotope ratio mass spectrometry (CF-IRMS; 20–20 SERCON mass spectrometer) after sample combustion to CO₂ and N₂ at 1000 °C in an on-line elemental analyzer (PDZEuropa ANCA-GSL). The precision, calculated by replicate analysis of an internal standard, was 0.05‰ for δ¹³C. The proportions and amounts of terrestrial and marine aquatic organic carbon were calculated from the TOC and δ¹³C data, using end-member values of –19.86‰ (Bertrand et al., 2012b) and –26.85‰ (this study; Appendix 1) for the aquatic and terrestrial sources, respectively.

A subset of 41 samples was analyzed for major and selected trace element geochemistry and carbonate content. Inorganic geochemistry was measured by ICP-AES following Bertrand et al. (2012b). In short, samples were prepared using the Li-metaborate fusion technique of Murray et al. (2000) and thirteen elements were measured on a JY Ultima C ICP-AES. Here, we report the concentrations of Ca and Sr. Analytical precision (1 σ) for these two elements, which was calculated from the analysis of ten individually-prepared sub-samples of reference sediment PACS-2, was 0.70% for Ca and 0.82% for Sr.

The weight percentage of total inorganic carbon (TIC) of the same subset of samples was determined using an UIC CM5012

coulometer equipped with a CM5130 acidification module. For each sample, 50–60 mg of sediment was precisely weighed into a Teflon cup, which was subsequently inserted into a glass tube and treated with 5 ml H_3PO_4 20% to liberate CO_2 . This method assumes that 100% of the measured CO_2 is derived from dissolution of calcium carbonate. The limit of detection was 0.04% CaCO_3 .

Lipids were extracted from the sediment samples according to the method of Bligh and Dyer (1959) but substituting chloroform with dichloromethane. Sediment samples were previously spiked with n-heptacosanone as a recovery standard. The lipid extracts were subjected to column chromatography and the fraction containing the C37 alkenones was concentrated and re-dissolved in isooctane with an internal standard (5- α -cholestane). Alkenones were analyzed on a Shimadzu Gas Chromatograph with a flame ionization detector (Prahil and Wakeham, 1987). C37 alkenones were identified by their retention times. The alkenone paleotemperature index (U^{K}_{37}) was calculated as $U^{K}_{37} = (\text{C37:2}) / (\text{C37:3} + \text{C37:2})$, where C37:2 and C37:3 represent the di- and triunsaturated C37 alkenones, respectively (Brassell et al., 1986). The U^{K}_{37} values were converted to sea surface temperature values by applying the calibration of Prahil and Wakeham (1987; $U^{K}_{37} = 0.033T + 0.043$). The analytical error was 7%.

Core chronology is based on ten carbonate shell fragments that were isolated for radiocarbon analysis (radiocarbon ages published in Boyd et al., 2008). No material suitable for dating was found below 932 cm. The age model was constructed with CLAM 2.2 (Blaauw, 2010) and it consisted in a smooth spline (smooth factor 0.35) running through the 10 calibrated radiocarbon ages. Calibration curve SHCal13 (Hogg et al., 2013) was used for the entire core and a variable reservoir age reflecting the evolution of the local environment from fresh to marine water was used ($R = 0$ before 9 cal kyr BP, $R = 270$ years between 9 and 8 cal kyr BP, and $R = 540$ years after 8 kyr cal BP; De Vleeschouwer et al. in prep.). In addition, the age model takes into account the instantaneous deposition of a turbidite at 1109–1096 cm and of the sand layers at 907–898 and 629–628 cm (Fig. 2).

In addition to sediment core JPC67, we also analyzed the geochemical composition of a river sediment sample (RS09-36) collected in 2009 in the outwash plain of the western branch of Marinelli glacier (Appendix 1; Fig. 1).

4. Results

4.1. Lithology and chronology

The 1345 cm-long sediment core is composed of grey to greyish olive organic-poor homogenous fine silt. It contains one turbidite at 1109–1096 cm and three sand layers at 1201–1200.5, 907–898 and 629–628 cm (Fig. 2). No clear tephra layers were observed, although it is possible that the turbidite and sand layers contain some tephra material (very low abundance of glass shards). According to the age model, the core covers the last 14,300 years and sedimentation rates vary between 0.4 and 0.8 mm/yr during the Holocene and reach up to 7 mm/yr during the deglaciation.

4.2. Physical properties

X-radiographs reveal abundant pebbles below 1100 cm and between 1030 and 875 cm, in addition to a few low-abundance intervals above 800 cm (Fig. 3). The concentration of IRD $>150 \mu\text{m}$ displays approximately the same trend, and both parameters are significantly positively correlated ($r = 0.55$; $p < 0.001$; Fig. 3).

The grain-size mode is relatively constant between 5 and 7 μm throughout the core, except for two intervals at 245–215 cm and

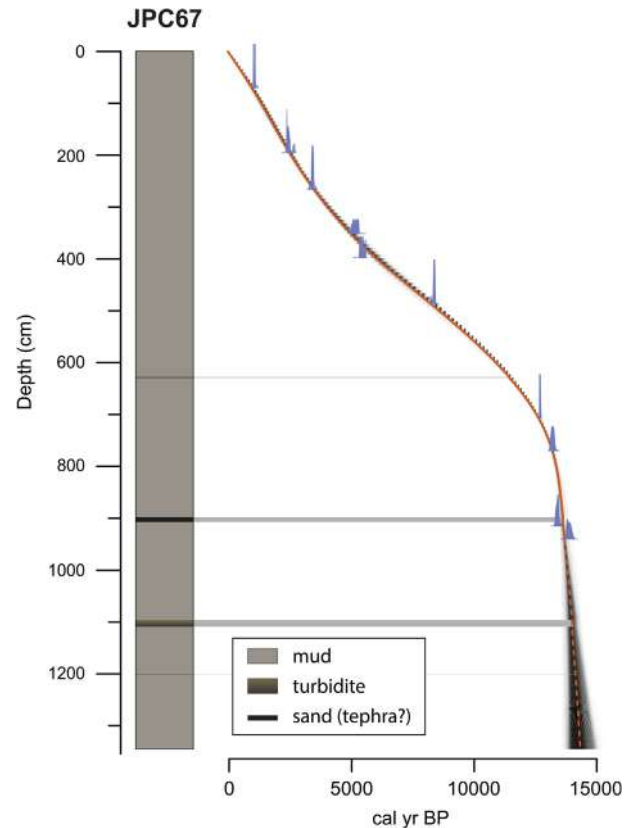


Fig. 2. Chronology of sediment core JPC67. The CLAM age model is based on the ten radiocarbon ages published in Boyd et al. (2008).

160–100 cm, where it reaches 8–9 μm (Fig. 3). The 1109–1096 cm turbidite and 907–898 cm sand layer also clearly stand out in the grain-size mode plot.

Throughout the core, the mass-specific and volume-specific MS values are highly positively correlated ($r = 0.93$; $p < 0.001$; Fig. 3), providing evidence that changes in sediment density have a minor influence on the higher-resolution volume-specific MS values. The main increases in MS are related to the coarser intervals at 245–215 cm and 160–100 cm. Relatively high MS values also occur at 490–475 cm, 400–285 cm, and in the upper 20 cm of the core, where no clear changes in grain-size mode are visible (Fig. 3).

4.3. Organic geochemistry

Total organic carbon concentrations are low throughout the core (between 0.2 and 1.2%), and they display a general increasing trend towards the upper part of the core (Fig. 4). The only two intervals where the TOC values deviate from the trend are at 245–215 cm and 155–110 cm, corresponding to the coarser samples (Fig. 3). The $\delta^{13}\text{C}$ data show a very similar trend, with enriched (more positive) $\delta^{13}\text{C}$ values when TOC increases. End-member modeling indicates that organic matter of terrestrial origin is always present and that most changes in TOC concentrations are due to variable amounts of carbon of marine origin (Appendix 2).

4.4. Inorganic geochemistry

XRF counts for halogen elements Br and Cl are used here to assess marine organic matter concentrations in sediments (Ziegler et al., 2008) and to estimate paleosalinity, respectively. In core JPC67, both elements display roughly the same trends as TOC and

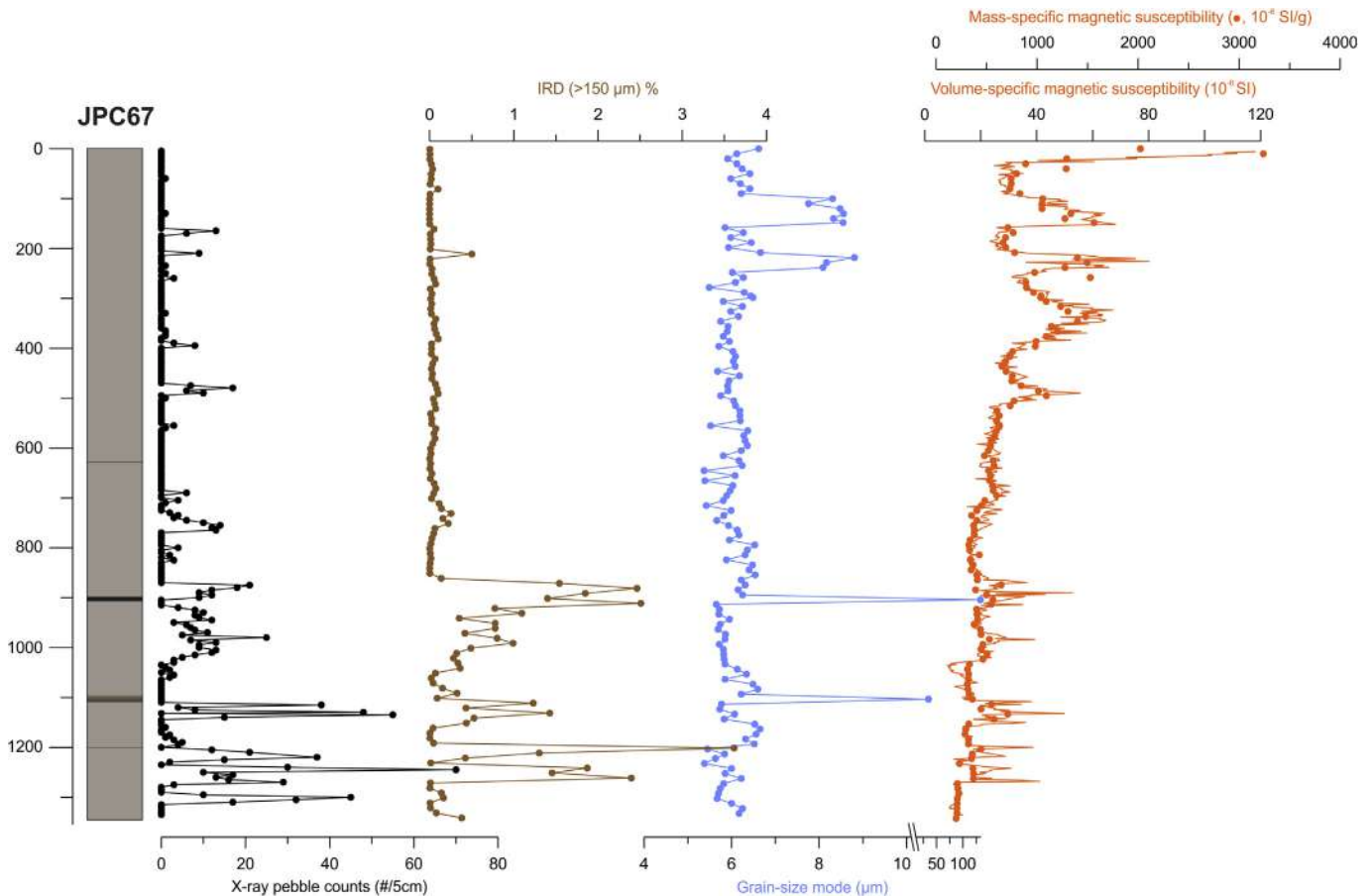


Fig. 3. Physical properties measured on sediment core JPC67. Note that magnetic susceptibility was measured both on the split core surface (volume-specific; 2 cm resolution) and on discrete samples (mass-specific; 10 cm resolution) to assess the influence of sediment density and water content on the high-resolution volume-specific measurements.

$\delta^{13}\text{C}$ (Fig. 4). The interpretation of Br counts as reflecting marine organic matter concentrations is confirmed by the significantly positive correlation between Br and marine OC ($r = 0.94$, $p < 0.001$). The similar trend in Cl counts suggests lower salinity conditions during the deposition of sediment with low marine organic matter concentrations.

Ca and Sr XRF counts are highly positively correlated to their concentrations measured by ICP-AES (Ca: $r = 0.90$, $p < 0.001$; Sr: $r = 0.96$, $p < 0.001$), showing that changes in physical properties have very little influence on Ca and Sr XRF core scanner intensities, in agreement with Bertrand et al. (2015). Both elements show a long-term increasing trend, punctuated by short-term increases in the coarser intervals at 245–215 cm and 155–110 cm, and in the upper 30 cm of the sediment core. The TIC values were below detection limit throughout the core, providing evidence that the sediment does not contain any carbonate, which in turn implies that Ca and Sr variations are related to the silicate fraction.

4.5. Alkenones

Alkenone concentrations were only measurable above 830 cm (Fig. 4). They were also below detection limit between 790 and 760 cm. In the rest of the core, alkenone concentrations are significantly positively correlated to the marine OC concentrations ($r = 0.59$, $p < 0.001$; Appendix 3). The calculated U^{K}_{37} SST values vary between 5 and 8 °C below 550 cm and average 10 ± 0.9 °C above, with the lowest values of the latter section occurring in the upper 30 cm of the sediment.

5. Discussion

5.1. Proxy interpretation

Many of the variables presented in Figs. 3 and 4 show clear co-variations. These variables can roughly be grouped in two main categories, which most certainly reflect two independent processes. The first category is defined by higher IRD, as suggested by pebble and $>150 \mu\text{m}$ particle counts. Intervals rich in IRD mostly occur at the bottom of the core, below 870 cm (Fig. 3). The second category is represented by sediments with a higher grain-size mode, which is also reflected in high MS values and Ca and Sr concentrations, in low marine organic carbon and alkenone concentrations, and in low Cl counts (Figs. 3 and 4; Appendix 2). The two main intervals showing these co-variations are located at 245–215 cm and 160–100 cm (Figs. 3 and 4).

Intervals with higher IRD are interpreted as reflecting the presence of glaciers calving in Almirantazgo fjord and/or in its tributary fjords and bays, which are able to produce icebergs and deliver coarse particles to coring site JPC67. Due to surface currents flowing towards the Northwest (Valdenegro and Silva, 2003), it is more likely that IRD originates from the glaciers calving in Parry fjord and Ainsworth Bay than in Brookes fjord (Fig. 1). However, although several glaciers are currently calving freely in Parry fjord, and producing icebergs, no IRD was detected in the most recent sediments of core JPC67. It is likely that icebergs calving in Parry fjord melt completely before they reach site JPC67, in agreement with our field observations. Likewise, shallow sills can create

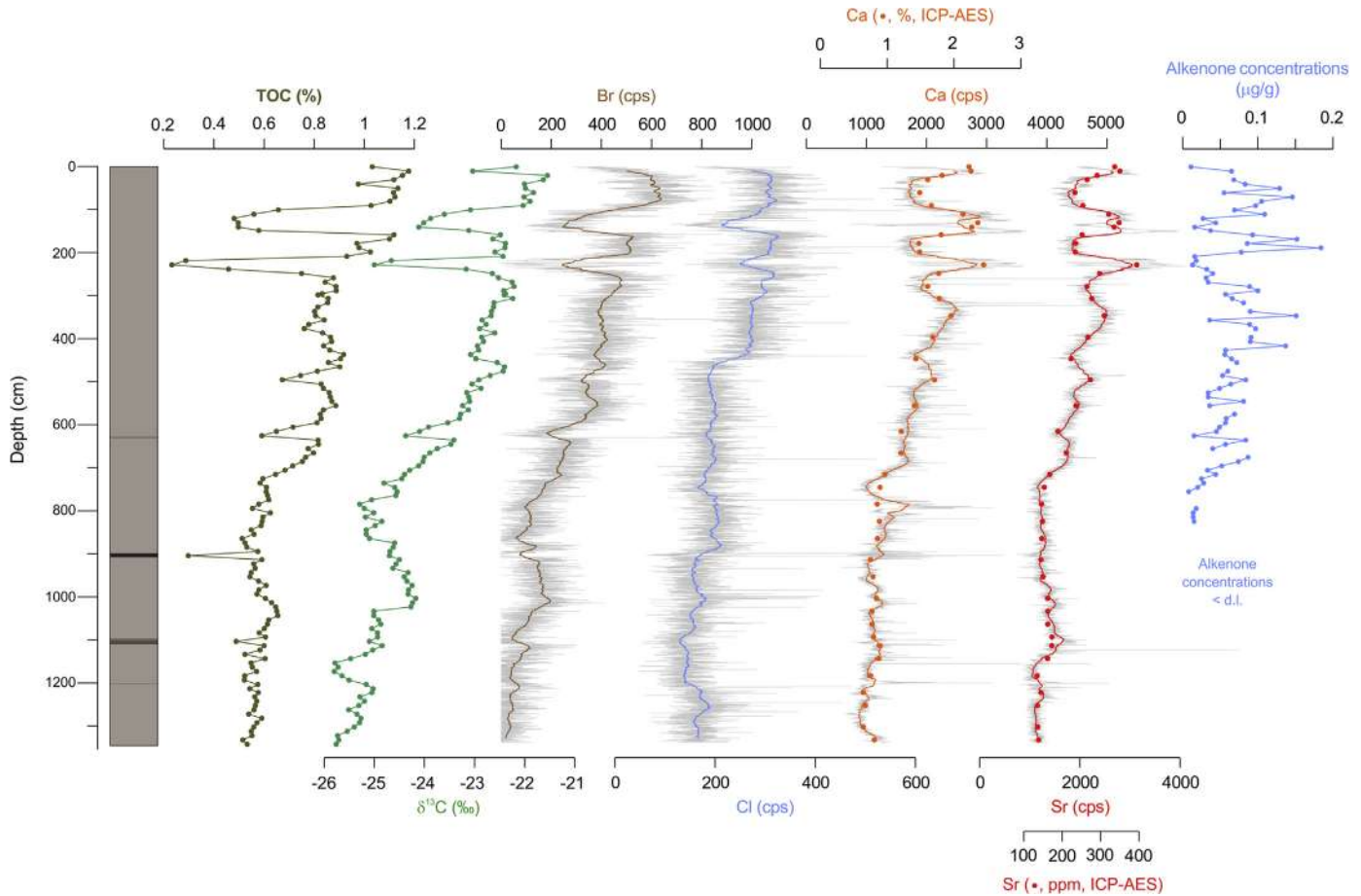


Fig. 4. Selected organic and inorganic geochemical parameters measured on sediment core JPC67. For the high-resolution XRF core scanner measurements (Br, Cl, Ca and Sr), the raw data (2 mm resolution) are presented in grey and the colored curves correspond to running averages over 20 cm (101 datapoints).

significant obstructions to the transport of icebergs, preventing them from drifting freely out of the fjord (Syvitski, 1989). The latter explains why IRD is absent from the most recent part of sediment core JPC67, while Marinelli glacier is currently calving and was producing high amounts of icebergs in the 1980s and 1990s (Porter and Santana, 2003). It appears that the shallow subaquatic arcuate moraine visible in Ainsworth bay (Fig. 1) is able to prevent icebergs from exiting the proximal basin, limiting their presence to the area between the current ice front and the arcuate moraine (Porter and Santana, 2003). Since this arcuate moraine formed during the LIA advance (Porter and Santana, 2003), it has no influence on pre-LIA IRD records. Therefore, IRD is mostly used here as an indicator of proximity to a calving glacier, instead of a simple proxy for the presence of calving glaciers.

Intervals with higher grain-size mode values, as observed at 245–215 cm and 160–100 cm (Fig. 3), are interpreted as periods of vigorous meltwater discharge. The coeval increases in MS and in Ca and Sr concentrations simply reflect the grain-size dependence of these three variables, as demonstrated by the results obtained on proglacial river sediment sample RS09-36 (Appendix 1). In RS09-36, MS, Ca, and Sr indeed peak in the fine and medium silt fractions, due to mineralogical sorting (Appendix 1). Since carbonate concentrations were always below detection limit, changes in Ca and Sr concentrations only reflect changes in the silicate fraction and their high concentrations seem to result from higher pyroxene abundance in fine and medium silts (Appendix 1). The interpretation of the higher grain-size mode values as representing vigorous meltwater discharge is confirmed by the concomitant decrease in

aquatic carbon of marine origin (Fig. 4; Appendix 2), representing dilution by a higher supply of terrigenous particles. In the two intervals at 245–215 cm and 160–100 cm, organic matter concentrations and stable isotopic composition are essentially the same as in Marinelli proglacial sediment sample RS09-36 (TOC = 0.43%; $\delta^{13}\text{C} = -26.85\text{‰}$; Fig. 4; Appendix 1), highlighting the predominantly terrestrial origin of the sediment in these two intervals. Our interpretation is further supported by the concomitant decrease in Cl XRF counts and by the extreme drop in alkenone concentrations (Fig. 4), indicating a freshening of the fjord waters.

5.2. Deglaciation

Following the interpretation of the sediment proxies in the previous section, the most indicative variables are presented versus age in Fig. 5. Sedimentation in core JPC67 starts at 14,300 cal yr BP with IRD-rich and organic-poor sediments interpreted as glacier-proximal deposits. Given that the core did not penetrate the entire sediment infill of Almirantazgo fjord (Boyd et al., 2008), the deglaciation of Almirantazgo fjord must have occurred prior to 14,300 cal yr BP, in agreement with Boyd et al. (2008) and with the recent hypothesis that CDI glaciers extensively retreated from their ultimate LGM advance during HS1 (18,000–14,600 cal yr BP; Hall et al., 2013). The existence of a glacier in Almirantazgo fjord until 15,500–11,700 cal yr BP, as suggested by McCulloch et al. (2005), is unlikely.

The high abundance of IRD, the absence of alkenones, and the very high sedimentation rates until 13,500 cal yr BP (Fig. 5) indicate

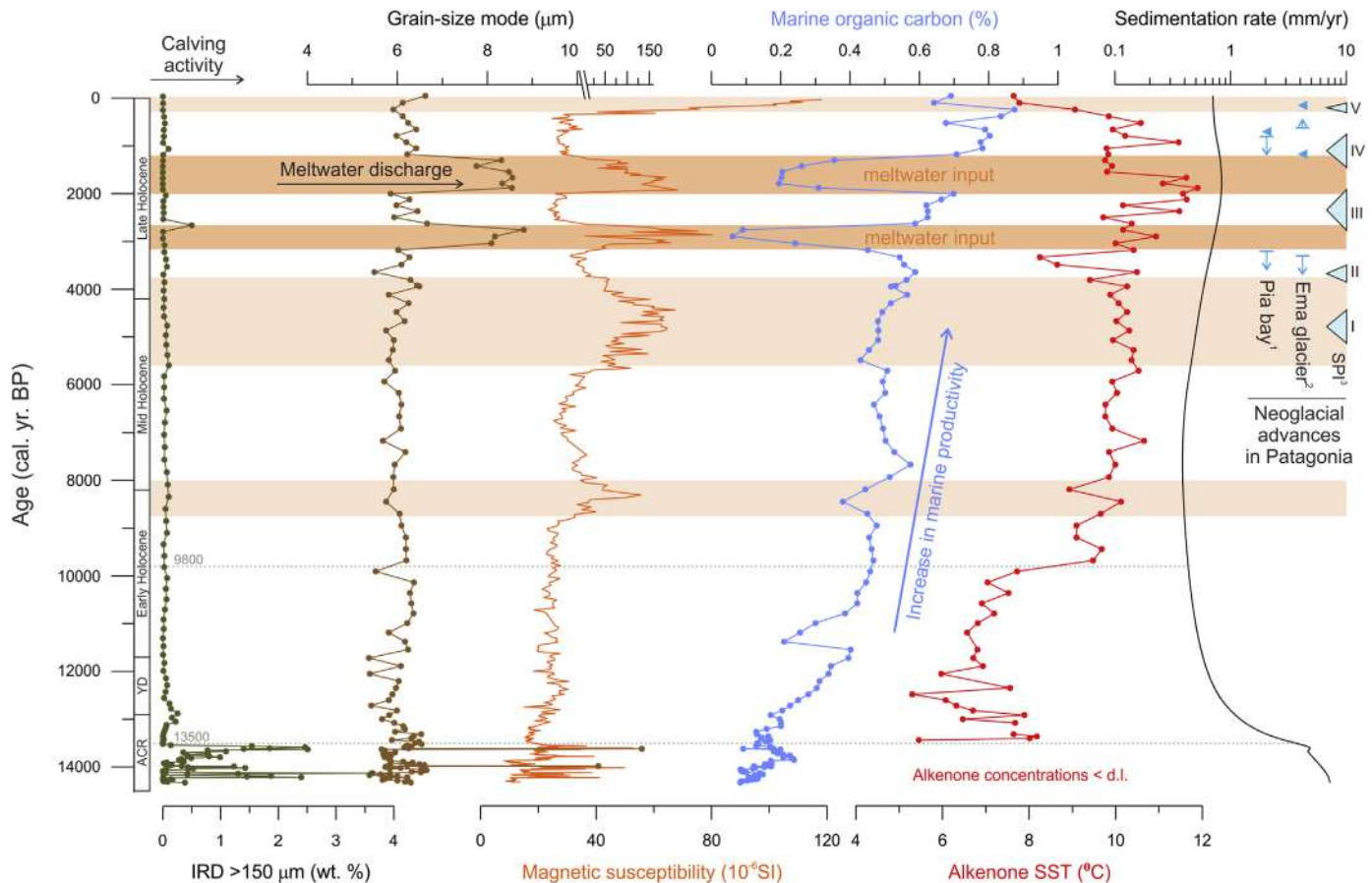


Fig. 5. Summary of the most indicative variables measured on sediment core JPC67 versus age. The horizontal orange rectangles represent meltwater intervals of proximal (dark) and more distal (light) glaciers. Neoglacial advances of CDI glaciers are indicated to the right of the figure: Pia bay from Kuylenstierna et al. (1996), and Ema glacier from Strelin et al. (2008). The five Neoglacial advances recognized for SPI glaciers by Aniya (2013) are also indicated. ACR and YD stand for Antarctic Cold Reversal and Younger Dryas, respectively. The sub-divisions of the Holocene are from Walker et al. (2012). (For interpretation of the references to colour in this figure legend, the reader is referred to the web version of this article.)

the presence of glaciers calving near coring site JPC67, as expressed by Boyd et al. (2008). At 13,500 cal yr BP, IRD disappears and alkenones start to be detected in the sediment (Fig. 5), indicating that the glaciers had shrunk significantly and that Almirantazgo fjord was an open fjord environment. The presence of high amounts of IRD immediately prior to 13,500 cal yr BP (Fig. 5) suggests that glaciers shrank due to rapid calving. Glaciers likely re-advanced slightly at 13,100–12,300 cal yr BP, as indicated by the presence of IRD, but certainly not as far as prior to 13,500 cal yr BP.

By 12,300 cal yr BP, ice fronts were likely near their present-day termini, in agreement with Boyd et al. (2008). Almirantazgo fjord, however, only became a predominantly saline fjord environment with near-modern oceanographic conditions by 9800 cal yr BP, as indicated by the significant increase in SST and – to a lesser extent – in organic carbon of marine origin (Fig. 5). This timing corresponds remarkably well to the early Holocene sea level rise (Fig. 6; Sidall et al., 2003; Smith et al., 2011) and likely reflects the arrival of warmer marine waters from the South Atlantic over the ~60m deep sill at Primera Angostura, as suggested by Aracena et al. (2015). After 9800 cal yr BP, Almirantazgo fjord became a typical marine fjord environment, affected by meltwater inputs from CDI glaciers.

5.3. Holocene variability of CDI outlet glaciers

During the last 9800 years, CDI outlet glaciers did not re-advance near their deglacial position. Although our Almirantazgo fjord

sediment record does not show any major IRD-rich interval during the Holocene, it clearly suggests the presence of two vigorous meltwater events at 3250–2700 and 2000–1200 cal yr BP, marked by clear increases in grain-size mode and MS, and by the substantial dilution of organic carbon of marine origin by detrital sediment input (Fig. 5). The latter interpretation is also confirmed by the general increase in sedimentation rates at ~3000–1000 cal yr BP (Fig. 5), which is likely due to the two events but could not be better temporally resolved due to the relatively low number of samples available for radiocarbon analysis in core JPC67. Interestingly, the sediment record shows the presence of low but significant amounts of IRD at 2700 cal yr BP, suggesting that some glaciers re-advanced to a calving position between the two melting events.

In addition to these two clearly-marked events, meltwater input may also have increased around 8750–8000 and 5600–3750 cal yr BP, as marked by higher MS values and slightly lower amounts of aquatic carbon of marine origin. The sedimentary signature of these two intervals is very similar to the variations observed for the last few decades, which are also marked by higher MS and slightly lower marine organic carbon concentrations, but for which no clear increase in grain size mode was observed (Fig. 5). The absence of variations in grain size likely reflects the trapping of sediment behind shallow sills in glacier-proximal basins, similar to what is currently occurring behind the arcuate LIA moraine of Marinelli glacier (Koppes et al., 2009).

During the last 9800 years, alkenone SSTs oscillate around 10 °C,

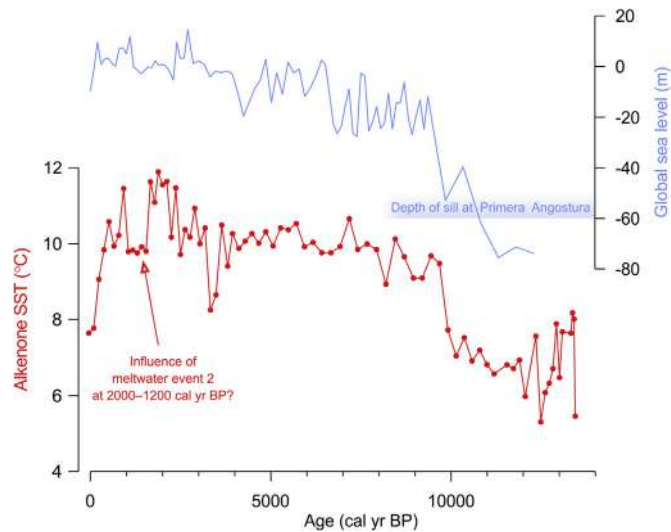


Fig. 6. Comparison between the alkenone SST values measured on sediment core JPC67 and the global sea-level rise curve of Siddal et al. (2003). The transgression from the South Atlantic likely occurred when sea level reached -60m , which corresponds to the depth of the sill at Primera Angostura in the Strait of Magellan.

although the exact values are much more variable after 4000 cal yr BP than before (Fig. 5). During the last 4000 years, particularly low values occur at 3500–3300 cal yr BP and during the most recent decades, and high values persisted between 2400 and 1600 cal yr BP. Since SSTs in fjord environments are influenced by marine water circulation and meltwater input, it is complicated to tell these two processes apart, but it is likely that the abrupt increases in SST around 3300–3200 and 2400–2200 cal yr BP participated in triggering the meltwater events at 3250–2700 and 2000–1200 cal yr BP, respectively. The subsequent abrupt drop in SST in 1600 cal yr BP likely represents the cooling of the fjord waters, with a slight delay, due to the increase in meltwater input. It is interesting to note that, although alkenones are similarly diluted by both meltwater events (Fig. 4; Appendix 3), SSTs only drop during/after the second event (Fig. 5), suggesting that the 2000–1200 cal yr BP meltwater event was larger in magnitude than its predecessor. Finally, the marked cooling of the last ~ 800 years may have very little to do with meltwater input and may rather represent the regional decrease in ocean temperatures during the last ~ 900 years (Caniupán et al., 2014).

5.4. Comparison with other glacier variability records in southernmost patagonia

Only two reconstructions of CDI glacier variability during the Holocene have been published. The first concerns glaciers reaching Pia bay, which is located on the southern flank of the icefield (Fig. 1), and it is based on radiocarbon-dated peat deposits developed in a former outwash plain (Kuylenstierna et al., 1996). The second consists of radiocarbon-dated moraine deposits in the Ema glacier valley (Monte Sarmiento; Fig. 1; Strelin et al., 2008).

In Pia bay, Kuylenstierna et al. (1996) identified three glacier maxima – before 3200 cal yr BP, prior to 800 cal yr BP and between 800 and 600 cal yr BP (Fig. 5). These glacier advances are entirely compatible with our Almirantazgo fjord sediment records since the first one occurs immediately prior to our first meltwater event at 3250–2700 cal yr BP, and later advances are posterior to our second meltwater event (Fig. 5).

The record of Strelin et al. (2008) suggests a possible glacier advance at 6800–5700 cal yr BP, and shows four well-marked

advances – shortly before 3300 cal yr BP, at 1170 cal yr BP, shortly after 620 cal yr BP and between 400 and 100 cal yr BP. The timing of the advance shortly before 3300 cal yr BP is strikingly similar to the advance in Pia bay before 3200 cal yr BP, and is therefore in good agreement with our record as well. It is noteworthy that these two advances correspond to the lowest SST in Almirantazgo fjord during the Holocene, suggesting that it may have been caused by a regional cooling. This cooling is however not reflected in the more marine records of Caniupán et al. (2014). The three advances that occurred after 1200 cal yr BP post-date our second meltwater event. The presence of low but significant amounts of IRD in our sediment record at 1100–1000 cal yr BP (Fig. 5) indicates that some of the northern CDI glaciers also re-advanced to a calving position after the second meltwater event.

An interesting observation is the apparent lack of glacier re-advance in Pia bay and in Ema glacier valley between 2700 and 2000 cal yr BP (i.e., between the two meltwater events identified in sediment core JPC67), although our sediment record shows the presence of IRD. One possible explanation is that the southern and western CDI glaciers responded differently to changes in climate, due to their orientation with respect to the southern westerly winds, as suggested by Holmund and Fuenzalida (1995).

Holocene variations in NPI and SPI glaciers have been studied in much more detail than for CDI glaciers. For the SPI, two schemes were proposed over the last decades (Glasser et al., 2004): the Mercer scheme, with three Neoglacial advances during the last 5000 years (Mercer, 1982); and the Aniya scheme with four advances during the same time interval (Aniya, 1995, 1996). In a recent review of Holocene SPI glacier advances, Aniya (2013) proposed a new scheme that combines the two previous chronologies. The latter contains five Neoglacial advances labeled from I to V at 5130–4430 cal yr BP, 3850–3490 cal yr BP, 2770–1910 cal yr BP, 1450–750 cal yr BP, and 350–50 cal yr BP (Fig. 5; ages calibrated from Aniya, 2013 using SHCal13). According to Aniya (2013), the most robust of these five advances, i.e., the intervals common to both original schemes, are advances III (2770–1910 cal yr BP) and V (17–19th centuries). The most recent findings of Strelin et al. (2014) and Kaplan et al. (2016) for the eastern side of the SPI are in general agreement with Aniya's chronology. Masiokas et al. (2009), however, suggested that in southern Patagonia, including Cordillera Darwin, the latest (LIA) advance could have occurred 1 to 3 centuries prior to the 19th century.

The timing of SPI advances II, IV and V corresponds reasonably well to the CDI advances described by Kuylenstierna et al. (1996) and Strelin et al. (2008) (Fig. 5). Although these authors did not describe any CDI glacier advance at 2770–1910 cal yr BP (Neoglacial advance III), our Almirantazgo sediment record suggests that Neoglacial advance III also affected CDI glaciers, providing evidence that CDI and eastern SPI glaciers varied in phase during most of the Neoglaciation. Only Neoglacial advance I does not seem to be recorded in any of the CDI records. In addition, it is important to note that our two vigorous meltwater events at 3250–2700 and 2000–1200 cal yr BP occur exactly in-between glacier advances II–III, and III–IV, respectively (Fig. 5). This observation suggests that CDI glaciers shrank and re-advanced rapidly during the late Holocene.

Prior to the Neoglaciation, the timing of SPI glacier advances is less consistent in the literature, with Aniya (2013) arguing for two possible advances at 8980–7610 (or 8270) cal yr BP and 6440–5680 cal yr BP, and Kaplan et al. (2016) describing an advance of eastern SPI glaciers at 6120 ± 390 cal yr BP. Although the latter may have occurred in the CDI as well, as suggested by Strelin et al. (2008; possible advance at 6800–5700 cal yr BP), our sediment record does not show any IRD during that time interval, suggesting that if glaciers indeed grew, their advance was less

extensive than during the Neoglaciation. The occurrence of very low MS values and of the lowest sedimentation rates of core JPC67 around 7300–5700 cal yr BP seems to confirm the absence of melting glaciers during that time interval. Therefore, it is likely that CDI glaciers were land-based and slightly advancing at 7300–5700 cal yr BP. Overall, however, CDI glaciers were much more stable during the first part of the Holocene than during the Neoglaciation.

5.5. Impact on surrounding aquatic and terrestrial environments

The meltwater events identified in sediment core JPC67 seem to have influenced nearby marine and terrestrial environments.

In sediment core MD07-3132, which is located in the central basin of the Strait of Magellan nearly 100 km to the northwest of JPC67 (Fig. 1), Aracena et al. (2015) described a period of particularly low carbonate productivity between 3200 and 2400 cal yr BP. This interval corresponds particularly well with the timing of the first meltwater event detected in sediment core JPC67 at 3250–2700 cal yr BP (Fig. 7). We suggest that, although productivity in the central basin of the Strait of Magellan was already low during the entire Neoglaciation, the first large CDI meltwater event at 3250–2700 cal yr BP put additional stress on carbonate organisms and reduced light penetration, causing fjord productivity to drop by a factor of three.

Similarly, outwash sediments are known to act as efficient dust sources, especially on glacial-interglacial timescales. Sugden et al. (2009), for example, showed that for the last 80,000 years, dust peaks in Antarctica coincided with periods of proglacial outwash sediment deposition in Patagonia. At the scale of the Holocene, Patagonian glacier variability also seems to affect dust production, as recently proposed by Vanneste et al. (2016). These authors identified relatively high dust accumulation rates in Karukinka, i.e., immediately across Almirantazgo fjord (Fig. 1) between 3100 and 1200 cal yr BP, peaking at 1900–1200 cal yr BP (Fig. 7). This peak

corresponds remarkably well to the timing of our second meltwater event at 2000–1200 cal yr BP, providing additional evidence that CDI glaciers retreated rather far landward at that time to allow the formation of extensive outwash plains. In addition, the onset of the increase in dust accumulation visible in the Karukinka peat record at 3100 cal yr BP coincides with the beginning of the first meltwater event. Therefore, we suggest that CDI glaciers shrank enough to form outwash plains during both meltwater events, but that glaciers shrank further during the second event, resulting in the formation of extensive outwash plains. These large exposed outwash plains provided fine-grained material available to be picked up by wind, as confirmed by the provenance study of Vanneste et al. (2016).

6. Conclusions

Sediment core JPC67 contains a continuous record of northern CDI glacier variability during the last 14,300 years. The age of the bottom of the core provides evidence that the deglaciation of Almirantazgo fjord occurred prior to 14,300 cal yr BP. The fjord remained a typical proglacial environment dominated by freshwater conditions until 9800 cal yr BP, with glacier-proximal conditions progressively disappearing after 13,500 cal yr BP. Almirantazgo fjord only became marine-dominated with oceanographic conditions similar to the present-day after the early Holocene sea-level rise at 9800 cal yr BP.

During the first half of the Holocene, our results show that glaciers were land-locked and relatively stable, except for a potential advance within land-based locations from 7300 to 5700 cal yr BP. In comparison, CDI glaciers re-advanced and shrank back much more rapidly during the Neoglaciation, and these variations were mostly in phase with eastern SPI glaciers. Of the five SPI Neoglacial advances described in the literature, only the first one (5130–4430 cal yr BP) is not expressed in Almirantazgo fjord sediments. In addition, our sediment record clearly shows that CDI outlet glaciers melted rapidly at 3250–2700 and 2000–1200 cal yr BP, but re-advanced to calving locations relatively soon afterwards (Neoglacial III and IV). These two melting events affected fjord productivity up to 100 km to the north of the CDI, and they exposed large outwash plains that acted as a source of dust for the Tierra del Fuego area, especially during the second event.

Our results highlight the potential of fjord sediments to reconstruct glacier variability at high resolution over multi-millennial timescales. Compared to traditional archives of glacier mass balance, they offer the advantage of continuously recording melting events and calving-land based transitions. We argue that fjord sediments should be increasingly used to reconstruct the evolution of mid and high-latitude glaciers, in addition to geomorphic mapping and exposure dating.

Acknowledgements

Cruise NBP0505 was funded by the National Science Foundation, Office of Polar Programs grant NSF/OPP 03-38137 to John Anderson and Julia Smith Wellner. The captain and crew of the RV/IB Nathaniel B. Palmer are acknowledged for their support during the cruise. We are grateful to Liviu Giosan (WHOI) and to Tim Ferdeman, Andrea Schipper and Thomas Max (MPI, Bremen) for providing access to the ITRAX XRF core scanner and UIC coulometer, respectively. We also warmly thank Reinout Debergh, Julian Janocha and Alvaro del Rey for processing some of the sediment samples for IRD and grain-size analysis during their studies at Ghent University. Brandi Boyd kindly provided the pebble count data and Lilian Núñez (UdeC) processed the sediment samples for alkenone analysis. Toon Van Dijck and Nathalie Fagel facilitated the

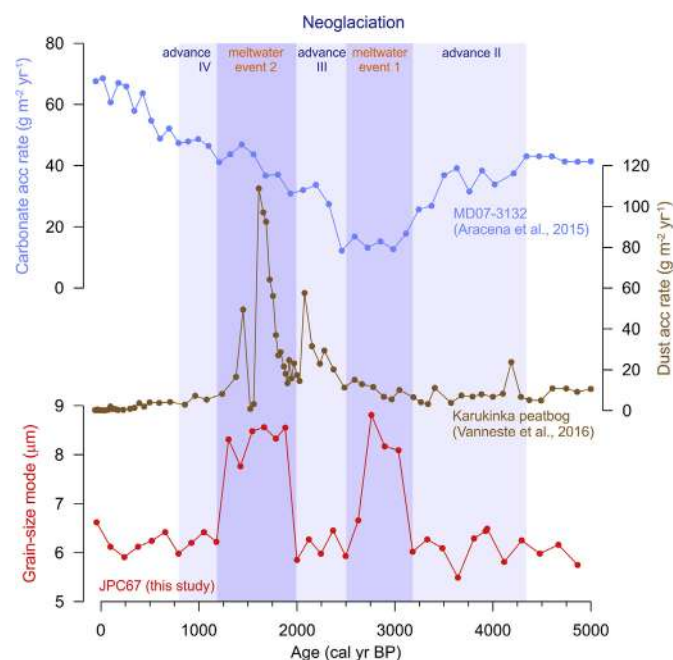


Fig. 7. Influence of rapidly shrinking CDI glaciers between Neoglacial advances II-III and III-IV on regional marine and terrestrial environments. Carbonate accumulation rates in sediment core MD07-3132 (central basin of the Strait of Magellan, see Fig. 1) are from Aracena et al. (2015), and the dust flux in Karukinka peatbog, which is located immediately across Almirantazgo fjord (Fig. 1), is from Vanneste et al. (2016).

acquisition of the XRD results presented in appendix. This research was supported by an EU Marie Curie FP6 postdoctoral fellowship to S.B., by National Geographic Grant 8379-07 (to S.B.), by COPAS Center FONDAP Grant 15010007 and COPAS Sur-Austral CONICYT PIA PFB31 (to C.L. and S.P.), and by IDEAL Center FONDAP Grant 15150003 (to C.L.). Samples were provided by the Antarctic Marine Geology Research Facility at Florida State University. We thank the facility curators for their assistance with shipping core JPC67 to WHOI. Finally, Mahyar Mohtadi (MARUM) and Rodrigo Fernandez (UT Austin) are thanked for constructive discussions at various stages of this project. One anonymous reviewer is acknowledged for providing valuable comments. The dataset presented in this article is available on PANGAEA: <https://doi.pangaea.de/10.1594/PANGAEA.881854>.

Appendix A. Supplementary data

Supplementary data related to this article can be found at <https://doi.org/10.1016/j.quascirev.2017.10.029>.

References

- Andresen, C.S., Straneo, F., Ribergaard, M.H., Björk, A.A., Andersen, T.J., Kuijpers, A., Nørgaard-Pedersen, N., Kjær, K.H., Schjøth, F., Weckström, K., Ahlström, A.P., 2011. Rapid response of Helheim Glacier in Greenland to climate variability over the past century. *Nat. Geosci.* 5, 37–41.
- Andrews, J.T., 2000. Icebergs and iceberg rafted detritus (IRD) in the North Atlantic: facts and assumptions. *Oceanography* 13, 100–108.
- Aniya, M., 1995. Holocene glacial chronology in Patagonia: Tyndall and Upsala glaciers. *Arct. Alp. Res.* 27 (4), 311–322.
- Aniya, M., 1996. Holocene variations of Ameghino Glacier, southern Patagonia. *Holocene* 6, 247–252.
- Aniya, M., 2013. Holocene glaciations of Hielo Patagonico (Patagonia Icefield), South America: a brief review. *Geochem. J.* 47, 97–105.
- Aracena, C., Kilian, R., Lange, C.B., Bertrand, S., Lamy, F., Arz, H.W., De Pol-Holz, R., Baeza, O., Pantoja, S., Kissel, C., 2015. Holocene variations in productivity associated with changes in glacier activity and freshwater flux in the central basin of the Strait of Magellan. *Palaeogeogr. Palaeoclimatol. Palaeoecol.* 436, 112–122.
- Bertrand, S., Hughen, K., Giosan, L., 2015. Limited influence of sediment grain size on elemental XRF core scanner measurements. In: Croudace, I.W., Rothwell, R.G. (Eds.), *Micro-XRF Studies of Sediment Cores*, pp. 473–490.
- Bertrand, S., Hughen, K.A., Lamy, F., Stuut, J.B.W., Torrejón, F., Lange, C.B., 2012a. Precipitation as the main driver of Neoglacial fluctuations of Gualas glacier, Northern Patagonian Icefield. *Clim. Past* 8, 519–534.
- Bertrand, S., Hughen, K.A., Sepúlveda, J., Pantoja, S., 2012b. Geochemistry of surface sediments from the fjords of Northern Chilean Patagonia (44–47°S): spatial variability and implications for paleoclimate reconstructions. *Geochimica Cosmochimica Acta* 76, 125–146.
- Blaauw, M., 2010. Methods and code for 'classical' age-modelling of radiocarbon sequences. *Quat. Geochronol.* 5, 512–518.
- Bligh, E.G., Dyer, W.J., 1959. A rapid method of total lipid extraction and purification. *J. Biochem. Physiology* 37, 911–917.
- Bown, F., Rivera, A., Zenteno, P., Bravo, C., Cawkwell, F., 2014. First glacier inventory and recent glacier variation on Isla Grande de Tierra del Fuego and adjacent Islands in Southern Chile. In: Kargel, J.S., Leonard, G.J., Bishop, M.P., Käab, A., Raup, B.H. (Eds.), *Global Land Ice Measurements from Space*, pp. 661–674.
- Boyd, B.L., Anderson, J.B., Wellner, J.S., Fernández, R.A., 2008. The sedimentary record of glacial retreat, Marinelli Fjord, Patagonia: regional correlations and climate ties. *Mar. Geol.* 255, 165–178.
- Brassell, S.C., Eglinton, G., Marlowe, I.T., Pflaumann, U., Sarnthein, M., 1986. Molecular stratigraphy: a new tool for climatic assessment. *Nature* 320, 129–133.
- Caniupán, M., Lamy, F., Lange, C.B., Kaiser, J., Arz, H., Kilian, R., Baeza Urrea, O., Aracena, C., Hebbeln, D., Kissel, C., Laj, C., Mollenhauer, G., Tiedemann, R., 2011. Millennial-scale sea surface temperature and Patagonian Ice Sheet changes off southernmost Chile (53°S) over the past ~60 kyr. *Paleoceanography* 26.
- Caniupán, M., Lamy, F., Lange, C.B., Kaiser, J., Kilian, R., Arz, H.W., León, T., Mollenhauer, G., Sandoval, S., De Pol-Holz, R., Pantoja, S., Wellner, J., Tiedemann, R., 2014. Holocene sea-surface temperature variability in the Chilean fjord region. *Quat. Res.* 82, 342–353.
- Davies, B.J., Glasser, N.F., 2012. Accelerating shrinkage of Patagonian glaciers from the Little Ice Age (~AD 1870) to 2011. *J. Glaciol.* 58, 1063–1084.
- Fernández, R., Gulick, S., Rodrigo, C., Domack, E., Leventer, A., 2017. Seismic stratigraphy and glacial cycles in the inland passages of the Magallanes region of Chile, southernmost South America. *Mar. Geol.* 386, 19–31.
- Fernández, R.A., Anderson, J.B., Wellner, J.S., Hallet, B., 2011. Timescale dependence of glacial erosion rates: a case study of Marinelli Glacier, Cordillera Darwin, southern Patagonia. *J. Geophys. Res. Earth Surf.* 116.
- Garreaud, R., Lopez, P., Minvielle, M., Rojas, M., 2013. Large-scale control on the Patagonian climate. *J. Clim.* 26, 215–230.
- Glasser, N.F., Harrison, S., Jansson, K.N., Anderson, K., Cowley, A., 2011. Global sea-level contribution from the Patagonian Icefields since the Little Ice age Maximum. *Nat. Geosci.* 4, 303–307.
- Glasser, N.F., Harrison, S., Winchester, V., Aniya, M., 2004. Late Pleistocene and Holocene palaeoclimate and glacier fluctuations in Patagonia. *Glob. Planet. Change* 43, 79–101.
- Grobe, H., 1987. A simple method for the determination of ice-rafted debris in sediment cores. *Polarforschung* 57, 123–126.
- Hall, B.L., Porter, C.T., Denton, G.H., Lowell, T.V., Bromley, G.R.M., 2013. Extensive recession of Cordillera Darwin glaciers in southernmost South America during Heinrich Stadial 1. *Quat. Sci. Rev.* 62, 49–55.
- Hogg, A.G., Hua, Q., Blackwell, P.G., Niu, M., Buck, C.E., Guilderson, T.P., Heaton, T.J., Palmer, J.G., Reimer, P.J., Reimer, R.W., Turney, C.S.M., Zimmerman, S.R.H., 2013. SHCal13 Southern Hemisphere calibration, 0–50,000 years cal BP. *Radiocarbon* 55, 1889–1903.
- Holmlund, P., Fuenzalida, H., 1995. Anomalous glacier responses to 20th century climatic changes in Darwin Cordillera, southern Chile. *J. Glaciol.* 41, 465–473.
- Howe, J.A., Austin, W.E.N., Forwick, M., Paetzel, M., 2010. Fjord Systems and Archives. Geological Society, London.
- Kaplan, M.R., Schaefer, J.M., Strelin, J.A., Denton, G.H., Anderson, R.F., Vandergoes, M.J., Finkel, R.C., Schwartz, R., Travis, S.G., Garcia, J.L., Martini, M.A., Nielsen, S.H.H., 2016. Patagonian and southern South Atlantic view of Holocene climate. *Quat. Sci. Rev.* 141, 112–125.
- Koppes, M., Hallet, B., Anderson, J., 2009. Synchronous acceleration of ice loss and glacial erosion, Glacier Marinelli, Chilean Tierra del Fuego. *J. Glaciol.* 55, 207–220.
- Koppes, M., Hallet, B., Rignot, E., Mougnot, J., Wellner, J.S., Boldt, K., 2015. Observed latitudinal variations in erosion as a function of glacier dynamics. *Nature* 526 (7571), 100–103.
- Kuijpers, A., Knutz, P., Moros, M., 2014. Ice-rafted debris (IRD). In: Harff, J., Meschede, M., Petersen, S., Thiede, J. (Eds.), *Encyclopedia of Marine Geosciences*, pp. 359–363.
- Kuylenstierna, J.L., Rosqvist, G.C., Holmlund, P., 1996. Late-Holocene glacier variations in the Cordillera Darwin, Tierra del Fuego, Chile. *Holocene* 6, 353–358.
- Lemke, P., Ren, J., Alley, R.B., Allison, I., Carrasco, J., Flato, G., Fujii, Y., Kaser, G., Mote, P., Thomas, R.H., Zhang, T., 2007. Observations: changes in snow, ice and frozen ground. In: Solomon, S., Qin, D., Manning, M., Chen, Z., Marquis, M., Averyt, K.B., Tignor, M., Miller, H.L. (Eds.), *Climate Change 2007: the Physical Science Basis. Contribution of Working Group I to the Fourth Assessment Report of the Intergovernmental Panel on Climate Change*. Cambridge University Press, Cambridge, United Kingdom and New York, NY, USA, pp. 337–383.
- Lenaerts, J.T.M., van den Broeke, M.R., van Wessem, J.M., van de Berg, W.J., van Meijgaard, E., van Ulf, L.H., Schaefer, M., 2014. Extreme precipitation and climate gradients in Patagonia revealed by high-resolution regional atmospheric climate modeling. *J. Clim.* 27, 4607–4621.
- Lopez, P., Chevallier, P., Favier, V., Pouyaud, B., Ordenes, F., Oerlemans, J., 2010. A regional view of fluctuations in glacier length in southern South America. *Glob. Planet. Change* 71, 85–108.
- Masiokas, M.H., Rivera, A., Espizua, L.E., Villalba, R., Delgado, S., Aravena, J.C., 2009. Glacier fluctuations in extratropical South America during the past 1000 years. *Palaeogeogr. Palaeoclimatol. Palaeoecol.* 281, 242–268.
- McCulloch, R.D., Fogwill, C.J., Sugden, D.E., Bentley, M.J., Kubik, P.W., 2005. Chronology of the last glaciation in central Strait of Magellan and Bahía Inútil, southernmost South America. *Geografiska annaler: series a. Phys. Geogr.* 87, 289–312.
- Melkonian, A.K., Willis, M.J., Pritchard, M.E., Rivera, A., Bown, F., Bernstein, S.A., 2013. Satellite-derived volume loss rates and glacier speeds for the Cordillera Darwin Icefield, Chile. *Cryosphere* 7, 823–839.
- Mercer, J.H., 1982. Holocene glacier variations in southern South America. *Striae* 18, 35–40.
- Moffat, C., 2014. Wind-driven modulation of warm water supply to a proglacial fjord, Jorge Montt Glacier, Patagonia. *Geophys. Res. Lett.* 41, 3943–3950.
- Murray, R., Miller, D., Kryc, K., 2000. Analysis of major and trace elements in rocks, sediments, and interstitial waters by inductively coupled plasma–atomic emission spectrometry (ICP–AES). *Odp. Tech. Note* 1–27.
- Porter, C., Santana, A., 2003. Rapid 20th century retreat of Ventisquero Marinelli in the Cordillera Darwin Icefield. *An. Del Inst. Patagon.* 31, 17–26.
- Prahl, F.G., Wakeham, S.G., 1987. Calibration of unsaturation patterns in long-chain ketone compositions for palaeotemperature assessment. *Nature* 330, 367–369.
- Rignot, E., Rivera, A., Casassa, G., 2003. Contribution of the Patagonia Icefields of South America to sea level rise. *Science* 302, 434–437.
- Sagredo, E., Lowell, T., 2012. Climatology of Andean glaciers: A framework to understand glacier response to climate change. *Global Planet. Change* 86–87, 101–109.
- Sernageomin, 2003. Mapa geológico de Chile versión digital, escala 1/1.000.000. SHOA, 1998. Bahía Inútil a Seno Almirantazgo y acceso Norte al Canal Magdalena. Mapa Batimétrico Escala 1/200.000.
- Siddall, M., Rohling, E.J., Almogi-Labin, A., Hemleben, C., Meischner, D., Schmelzer, I., Smeed, D.A., 2003. Sea-level fluctuations during the last glacial cycle. *Nature* 423, 853–858.
- Smith, D.E., Harrison, S., Firth, C.R., Jordan, J.T., 2011. The early Holocene sea level rise. *Quat. Sci. Rev.* 30, 1846–1860.
- Strelin, J., Casassa, G., Rosqvist, G., Holmlund, P., 2008. Holocene glaciations in the

- Ema Glacier valley, Monte Sarmiento Massif, Tierra del Fuego. *Palaeogeogr. Palaeoclimatol. Palaeoecol.* 260, 299–314.
- Strelin, J.A., Kaplan, M.R., Vandergoes, M.J., Denton, G.H., Schaefer, J.M., 2014. Holocene glacier history of the Lago Argentino basin, Southern Patagonian Icefield. *Quat. Sci. Rev.* 101, 124–145.
- Sugden, D.E., McCulloch, R.D., Bory, A.J.M., Hein, A.S., 2009. Influence of Patagonian glaciers on Antarctic dust deposition during the last glacial period. *Nat. Geosci.* 2, 281–285.
- Syvitski, J.P.M., 1989. On the deposition of sediment within glacier-influenced fjords - oceanographic controls. *Mar. Geol.* 85, 301–329.
- Valdenegro, A., Silva, N., 2003. Caracterización oceanográfica física y química de la zona de canales y fiordos australes de Chile entre el estrecho de Magallanes y cabo de Hornos (Cimar 3 Fiordos). *Cienc. Tecnol. Del Mar* 26, 19–60.
- Vanneste, H., De Vleeschouwer, F., Bertrand, S., Martínez-Cortizas, A., Vanderstraeten, A., Mattielli, N., Coronato, A., Piotrowska, N., Jeandel, C., Roux, G.L., 2016. Elevated dust deposition in Tierra del Fuego (Chile) resulting from Neoglacial Darwin Cordillera glacier fluctuations. *J. Quat. Sci.* 31, 713–722.
- Verardo, D.J., Froelich, P.N., Mcintyre, A., 1990. Determination of organic carbon and nitrogen in marine sediments using the Carlo Erba NA-1500 analyzer. *Deep-Sea Res.* 37, 157–165.
- Walker, M.J.C., Berkelhammer, M., Björck, S., Cwynar, L.C., Fisher, D.A., Long, A.J., Lowe, J.J., Newnham, R.M., Rasmussen, S.O., Weiss, H., 2012. Formal subdivision of the Holocene series/epoch: a discussion paper by a working group of INTIMATE (integration of ice-core, marine and terrestrial records) and the sub-commission on quaternary stratigraphy (international commission on stratigraphy). *J. Quat. Sci.* 27, 649–659.
- Ziegler, M., Jilbert, T., de Lange, G.J., Lourens, L.J., Reichert, G.-J., 2008. Bromine counts from XRF scanning as an estimate of the marine organic carbon content of sediment cores. *Geochemistry, Geophysics, Geosystems* 9.